

Fatigue crack growth simulations of interfacial cracks in bi-layered FGMs using XFEM

S. Bhattacharya · I. V. Singh · B. K. Mishra ·
T. Q. Bui

Received: 31 August 2012 / Accepted: 14 February 2013 / Published online: 6 March 2013
© Springer-Verlag Berlin Heidelberg 2013

Abstract An investigation of fatigue crack growth of interfacial cracks in bi-layered materials using the extended finite element method is presented. The bi-material consists of two layers of dissimilar materials. The bottom layer is made of aluminium alloy while the upper one is made of functionally graded material (FGM). The FGM layer consists of 100 % aluminium alloy on the left side and 100 % ceramic (alumina) on the right side. The gradation in material property of the FGM layer is assumed to be exponential from the alloy side to the ceramic side. The domain based interaction integral approach is extended to obtain the stress intensity factors for an interfacial crack under thermo-mechanical load. The edge and centre cracks are taken at the interface of bi-layered material. The fatigue life of the interface crack plate is obtained using the Paris law of fatigue crack growth under cyclic mode-I, mixed-mode and thermal loads. This study reveals that the crack propagates into the FGM layer under all types of loads.

Keywords Bi-layered FGM · Interface crack ·
Extended finite element method ·
Fatigue crack propagation

1 Introduction

Dissimilar or layered materials such as ceramic-metal and composite-metal have been widely used in engineering

applications for the purpose of increasing the strength and reducing the weight simultaneously. The structural performance of layered material depends on the mechanical properties and the fracture behavior of the interface. Unlike the behavior of homogeneous materials, abrupt change in material properties at the interface is the primary source of failure in layered materials. Flaws or defects in the material like micro-cracks or pores can complicate the modeling of layered materials. These features should be taken into account for the appropriate modeling of the structure/component. The fracture failure of a component is always preceded by multi-site cracks. The crack tip stress fields of all such cracks interact with one another, and this interaction results in the formation of one dominant crack which leads to the final failure of the component. Hence, accurate evaluation of stress intensity factors is essential for the prediction of failure and crack growth rate in these components.

In recent years, functionally graded materials (FGMs) are used as an alternative material to the conventional homogeneous coatings. FGMs are composite materials in which the composition or microstructure or both are locally varied so that specified variation of the local material properties can be achieved. FGMs are found to be quite attractive for the application in variety of thermal shielding problems including high temperature chambers, furnace liners, gas turbines, micro-electronics and space structures. The design of components involving FGMs and guarding them against fracture failure becomes an important issue. The fatigue and fracture characterization of such materials require the solution of certain standard crack problems. The crack problems solved over the past few decades in nonhomogeneous materials provide some valuable knowledge for the fracture mechanics research on FGMs, and reveal the considerable developments in exploring the fracture behavior of bi-layered materials. Sukumar et al. [22] developed a partition of unity enrichment

S. Bhattacharya · I. V. Singh (✉) · B. K. Mishra
Department of Mechanical and Industrial Engineering, IIT,
Roorkee, India
e-mail: ivsingh@gmail.com

T. Q. Bui
Department of Civil Engineering, University of Siegen,
Siegen, Germany

technique for bi-material interface cracks. They added a discontinuous function and near-tip asymptotic displacement functions in the finite element approximation obtained from the displacement fields for an interfacial crack. Liu et al. [8] improved the extended finite element method (XFEM) to directly evaluate mixed-mode stress intensity factors without extra post-processing for homogeneous materials as well as for bi-materials. Rethore et al. [18] demonstrated that the enrichment functions in XFEM can give more accurate and stable numerical scheme for crack growth simulations, and also [19] presented a time partition of the unity scheme based on Newmark method for the simulation of dynamic crack propagation. Walters et al. [23] used the FEM to compute the mixed-mode stress intensity factors for cracks in 3-D FGMs. Nagai et al. [12] developed a finite element based numerical approach to evaluate the SIFs of a 3-D interface crack between dissimilar anisotropic materials. Qin et al. [15] calculated the mixed-mode stress intensity factors of a 3-D interfacial crack in bi-material under shear loading using hypersingular integral equation method. Zhu et al. [26] used hypersingular integro-differential equation method for solving the 3-D interface crack in fully coupled electromagnetoelastotropic anisotropic multiphase composites under extended electromagnetoelastropic coupled loads. Yu et al. [24] investigated the interface crack between two nonhomogeneous materials. They developed a new interaction energy integral for obtaining mixed mode stress intensity factors of an interface crack between two nonhomogeneous materials with continuous or discontinuous properties. They also used this approach [25] to evaluate the SIFs for 3-D curved cracks in nonhomogeneous materials. Pant et al. [13] implemented the element free Galerkin method (EFGM) for the stress analysis of structures having cracks at the interface of two dissimilar materials. They modeled the material discontinuity at the interface using a jump function and jump parameter that governs its strength. Menshykov et al. [9] solved the 3-D dynamic problems of elastic bi-materials with cracks located at the bonding interface under harmonic loading. Guo et al. [5] analyzed a plane crack problem of nonhomogeneous materials with interfaces subjected to static thermal loading. They developed a modified interaction energy integral method to obtain the mixed-mode thermal stress intensity factors. Pathak et al. [14] simulated bi-material interfacial cracks using EFGM and XFEM under mode-I and mixed-mode loading conditions. From the literature, it can be inferred that the fatigue behaviour of such problems has not been investigated to date. Moreover, the thermal and mixed-mode fatigue problems have not been explored as well. Therefore, in this work, the fatigue life of bi-material interfacial cracks is estimated by the XFEM under mode-I, mixed-mode and thermal fatigue loads. The crack growth is modeled using

level sets. A major crack is incorporated at the edge as well as at the centre of the domain at the interface of bi-materials. Cyclic mode-I, mixed-mode and thermal loads are applied and the number of cycles to failure with crack extension under each type of loading is estimated using Paris equation. In addition, crack propagation paths are also presented to depict the nature of fatigue behaviour under various types of loading.

XFEM formulation for an interfacial crack is presented in Sect. 2. Section 3 depicts a detailed methodology of SIF calculation based on interaction integral approach. The fatigue crack growth phenomenon in the bi-layered plate is explained in Sect. 4. Section 5 describes the physics of the FGM along with its relevant properties. Section 6 describes the problem description, results and discussions whereas Sect. 7 present the conclusions derived from the present study.

2 XFEM formulation for FGM

XFEM is a partition of unity (PU) enriched finite element method. PU is quite useful for obtaining the solutions of the problems with prominent non-smooth characteristics in the small parts of the computational domain like discontinuities and singularities. In XFEM, a crack is modeled by enrichment functions so a regular mesh can be used for modeling the crack and crack growth without altering the initial mesh. It also eliminates the need of singular or Barsoum elements for capturing the singularity at the crack tip (as required in the standard FEM). In XFEM, standard FEM approximation is enriched by crack tip functions derived from the displacement solution of a linear elastic crack. In this method, the mesh remains independent of crack location so there is no issue like tracking the time history of points as required in standard FEM. Moreover, a higher degree of accuracy can be achieved with the less number of data points. A detailed XFEM formulation for the FGM is provided in “Appendix A”.

3 Computation of stress intensity factors for FGM

The domain based interaction integral approach has been widely used for calculating the stress intensity factors for homogeneous, bi-material and functionally graded materials under thermal and mechanical loads [1, 5, 7, 16]. In the present study, an interaction integral approach is extended to calculate the stress intensity factors for bi-layered FGMs under thermal and mechanical loads. The interaction integral M_{12} can be defined as

$$M_{12} = \int_{A_o} \left(\sigma_{ij} \frac{\partial u_i^a}{\partial x_1} + \sigma_{ij}^a \frac{\partial u_i}{\partial x_1} - \sigma_{ik}^a \varepsilon_{ik}^m \delta_{1j} \right) \frac{\partial q}{\partial x_j} dA + \int_{A_o} \left(\sigma_{ij} (S_{ijkl}^{tip} - S_{ijkl}(\mathbf{x})) \frac{\partial \sigma_{kl}^a}{\partial x_1} + \sigma_{ij}^a \left(\frac{\partial \gamma}{\partial x_1} \Delta T + \gamma \frac{\partial \Delta T}{\partial x_1} \right) \delta_{ij} \right) q dA \tag{1}$$

where superscript *a* represents the auxiliary state, superscript *m* denotes the mechanical component, *q* is a weight function which is *one* at the inner path Γ_1 , zero at the outer path Γ_2 , and arbitrary elsewhere, and γ is the coefficient of thermal expansion. For mode-I and mixed-mode loadings, term ΔT in Eq. (1) reduces to zero. Thus, Eq. (1) reduces to

$$M_{12} = \int_{A_o} \left(\sigma_{ij} \frac{\partial u_i^a}{\partial x_1} + \sigma_{ij}^a \frac{\partial u_i}{\partial x_1} - \sigma_{ik}^a \varepsilon_{ik}^m \delta_{1j} \right) \frac{\partial q}{\partial x_j} dA + \int_{A_o} \left(\sigma_{ij} (S_{ijkl}^{tip} - S_{ijkl}(\mathbf{x})) \frac{\partial \sigma_{kl}^a}{\partial x_1} \right) q dA \tag{2}$$

In case of aluminum alloy (homogeneous material), $S_{ijkl}^{tip} = S_{ijkl}(\mathbf{x})$. Thus, Eq. (2) reduces to

$$M_{12} = \int_{A_o} \left(\sigma_{ij} \frac{\partial u_i^a}{\partial x_1} + \sigma_{ij}^a \frac{\partial u_i}{\partial x_1} - \sigma_{ik}^a \varepsilon_{ik}^m \delta_{1j} \right) \frac{\partial q}{\partial x_j} dA \tag{3}$$

For bi-material interfacial cracks, the auxiliary fields [24,25] used in Eq. (1) can be written as

$$u_i^a = \left\{ \begin{array}{l} \frac{\tilde{f}_i^I(r, \theta, \varepsilon^{tip}, \kappa_{\tilde{m}}^{tip})}{4\mu_{\tilde{m}}^{tip} \cosh(\pi \varepsilon^{tip})} \sqrt{\frac{r}{2\pi}} \text{ for } K_I^a = 1, K_{II}^a = 0 \\ \frac{\tilde{f}_i^{II}(r, \theta, \varepsilon^{tip}, \kappa_{\tilde{m}}^{tip})}{4\mu_{\tilde{m}}^{tip} \cosh(\pi \varepsilon^{tip})} \sqrt{\frac{r}{2\pi}} \text{ for } K_I^a = 0, K_{II}^a = 1 \end{array} \right\} \tag{4}$$

with $i = 1, 2$ and $\tilde{m} = 1, 2$

where $\tilde{m} = 1$ indicates material *m*1 or FGM1, $\tilde{m} = 2$ indicates material *m*2 or FGM2 and Roman superscript I and II on the function \tilde{f} indicate mode-I and mode-II.

$\varepsilon^{tip} = \frac{1}{2\pi} \ln \left(\frac{\kappa_1^{tip}/\mu_1^{tip} + 1/\mu_2^{tip}}{\kappa_2^{tip}/\mu_2^{tip} + 1/\mu_1^{tip}} \right)$. $\mu_{\tilde{m}}^{tip}$ is the shear modulus of material \tilde{m} at the crack tip and $\kappa_{\tilde{m}}^{tip}$ is the Kolosov coefficient of the material \tilde{m} at the crack tip defined as $\kappa_{\tilde{m}}^{tip} = \frac{(3-\nu_{\tilde{m}}^{tip})}{(1+\nu_{\tilde{m}}^{tip})}$

for plane stress, $\kappa_{\tilde{m}}^{tip} = 3 - 4\nu_{\tilde{m}}^{tip}$ for plane strain where $\nu_{\tilde{m}}^{tip}$ is the Poisson’s ratio of material \tilde{m} at the crack tip. The functions \tilde{f}_i^I and \tilde{f}_i^{II} can be given as

$$\tilde{f}_1^I = \tilde{D} + \tilde{T}_1, \tilde{f}_2^I = -\tilde{C} - \tilde{T}_2, \tilde{f}_1^{II} = -\tilde{C} + \tilde{T}_2 \text{ and } \tilde{f}_2^{II} = -\tilde{D} + \tilde{T}_1 \tag{5a}$$

where \tilde{C} , \tilde{D} , \tilde{T}_1 and \tilde{T}_2 are

$$\tilde{C} = \tilde{\beta}' \tilde{\gamma} \cos \frac{\theta}{2} - \tilde{\beta} \tilde{\gamma}' \sin \frac{\theta}{2}, \tilde{D} = \tilde{\beta} \tilde{\gamma} \cos \frac{\theta}{2} + \tilde{\beta}' \tilde{\gamma}' \sin \frac{\theta}{2}, \tag{5b}$$

$$\tilde{T}_1 = 2\tilde{\delta} \sin \theta \sin \tilde{\phi}, \tilde{T}_2 = 2\tilde{\delta} \sin \theta \cos \tilde{\phi} \tag{5c}$$

$$\tilde{\beta} = \frac{\frac{1}{2} \cos(\varepsilon^{tip} \ln(r)) + \varepsilon^{tip} \sin(\varepsilon^{tip} \ln(r))}{\frac{1}{4} + (\varepsilon^{tip})^2}, \tilde{\beta}' = \frac{\frac{1}{2} \sin(\varepsilon^{tip} \ln(r)) - \varepsilon^{tip} \cos(\varepsilon^{tip} \ln(r))}{\frac{1}{4} + (\varepsilon^{tip})^2} \tag{5d}$$

$$\tilde{\gamma} = \kappa^{tip} \tilde{\delta} - \frac{1}{\tilde{\delta}}, \tilde{\gamma}' = \kappa^{tip} \tilde{\delta} + \frac{1}{\tilde{\delta}} \tag{5e}$$

In above equations, $\tilde{\phi}$, κ^{tip} and $\tilde{\delta}$ can be obtained as

$$\tilde{\phi} = \varepsilon^{tip} \ln(r) + \frac{\theta}{2}, \kappa^{tip} = \begin{cases} \kappa_1^{tip} (x_2 > 0) \\ \kappa_2^{tip} (x_2 < 0) \end{cases}, \tilde{\delta} = \begin{cases} e^{(\theta-\pi)} \varepsilon^{tip} (x_2 > 0) \\ e^{(\theta+\pi)} \varepsilon^{tip} (x_2 < 0) \end{cases} \tag{5f}$$

The stresses and strains are evaluated as

$$\sigma_{ij}^a = C_{ijkl}^{tip} \varepsilon_{kl}^a = C_{ijkl}^{tip} (u_{k,l}^a + u_{l,k}^a)/2 \text{ and } \varepsilon_{ij}^a = S_{ijkl}(\mathbf{x}) \sigma_{kl}^a \text{ for } i, j, k, l = 1, 2 \tag{6}$$

Thus, the numerical evaluation of interaction integral enables us to compute the mixed-mode SIFs. For bi-layered problems, the SIFs are calculated from the interaction integral as Yu et al. [24,25]:

$$K_I = \frac{M_{12} E^* \cosh^2(\pi \varepsilon^{tip})}{2} \text{ with } K_I^a = 1 \text{ and } K_{II}^a = 0 \tag{7a}$$

$$K_{II} = \frac{M_{12} E^* \cosh^2(\pi \varepsilon^{tip})}{2} \text{ with } K_I^a = 0 \text{ and } K_{II}^a = 1 \tag{7b}$$

where $E^* = \frac{2\bar{E}_1 \bar{E}_2}{\bar{E}_1 + \bar{E}_2}$ with

$$\bar{E}_i = \begin{cases} E_i^{tip} & \text{for plane stress} \\ E_i^{tip} / (1 - (\nu_i^{tip})^2) & \text{for plane strain} \end{cases} \text{ with } i = 1, 2$$

A detailed derivation of the interaction integral M_{12} is given in “Appendix B”.

4 Fatigue crack growth

In the present work, Paris law is used to find the rate of crack growth. For an applied thermo-mechanical load, the SIFs corresponding to the maximum and the minimum load can be evaluated using the approach outlined in the last section. At each crack tip, the local direction of crack growth θ_c is

determined on the basis of maximum principal stress theory [21]. The crack is assumed to grow in a direction perpendicular to the maximum principal stress. According to this criterion, the equivalent mode-I SIF and crack growth direction are given as

$$K_{Ieq} = K_I \cos^3\left(\frac{\theta_c}{2}\right) - 3K_{II} \cos^2\left(\frac{\theta_c}{2}\right) \sin\left(\frac{\theta_c}{2}\right) \quad (8)$$

$$\theta_c = 2 \tan^{-1} \left(\frac{K_I - \sqrt{K_I^2 + 8K_{II}^2}}{4K_{II}} \right) \quad (9)$$

Equation (9) gives two values of θ_c . One of these values corresponds to maximum and the other corresponds to a minimum. θ_c corresponding to the maximum equivalent SIF can be found as

$$\Delta K_{Ieq} = \Delta K_I \cos^3\left(\frac{\theta_c}{2}\right) - 3\Delta K_{II} \cos^2\left(\frac{\theta_c}{2}\right) \sin\left(\frac{\theta_c}{2}\right) \quad (10)$$

The values of θ_c and ΔK_{Ieq} obtained using Eqs. (9) and (10) will pertain to one of the materials of the bi-layer. For the other material, the maximum ΔK_{Ieq} will be equal to ΔK_I only and the corresponding angle will be $\theta = 0$. In this way, ΔK_{Ieq} and the possible crack propagation direction may be found for both the materials. In the present work, ΔK_{Ieq} in both the materials is compared against their respective local fracture toughness to decide the material in which the crack growth will take place. Thus, ratios R_1 and R_2 are defined as

$$R_1 = \frac{(\Delta K_{Ieq})_{m1}}{(K_{IC})_{m1}} \text{ and } R_2 = \frac{(\Delta K_{Ieq})_{m2}}{(K_{IC})_{m2}} \quad (11)$$

where $m1$ and $m2$ signify material-1 and material-2 of the bi-layer. If $R_1 > R_2$ then the crack propagates in the first material along $\theta = \theta_c$ otherwise it propagates in the other material along the interface ($\theta = 0$).

For stable crack propagation, the generalized Paris' law is given as

$$\frac{da}{dN} = C(\mathbf{x}) (\Delta K_{Ieq})^{m(\mathbf{x})} \quad (12)$$

where $C(\mathbf{x})$ and $m(\mathbf{x})$ are the functions of the location.

In the numerical implementation, a value of crack growth Δa is assumed and the corresponding number of cycles ΔN is calculated from Eq. (12). When more than one crack tip is present, Δa for the most dominant crack tip is assumed, corresponding ΔN is calculated and then the crack growth at the other crack tips are calculated corresponding to this known value of ΔN . Finally, when the maximum value of K_{Ieq} for any crack tip becomes more than the local value of the fracture toughness K_{IC} then the simulation is stopped. At this point, the total number of cycles elapsed is the fatigue life of the FGM.

5 Variation in the properties of FGM

In the present work, the results have been presented for a bi-layered plate consisting of FGM in the upper half and aluminium alloy in the lower half as shown in Fig. 1a, b. The FGM layer is composed of aluminum alloy and alumina. The volume fraction of alumina is varied in x -direction to obtain the gradation in material property. It is assumed that the FGM has the properties of the aluminum alloy at $x = 0$ and ceramic (alumina) at $x = L$. The crack is taken along the interface of bi-layered material. The material properties of the aluminum alloy and alumina are tabulated in Table 1. The variation of the elastic modulus for FGM is modeled as

$$E(x) = E_{alloy} e^{\alpha x} \text{ where } \alpha \text{ is given as} \quad (13)$$

$$\alpha = \frac{1}{L} \ln \left(\frac{E_{ceramic}}{E_{alloy}} \right)$$

Further, it is assumed that the local elastic modulus of the FGM can be obtained by applying the rule of mixture with the local volume fraction of alumina. Then, the volume fractions of ceramic and aluminum alloy in the FGM are obtained as

$$V_{ceramic}^{FGM}(x) = \frac{E(x) - E_{alloy}}{E_{ceramic} - E_{alloy}} = \frac{E_{alloy} e^{\alpha x} - E_{alloy}}{E_{ceramic} - E_{alloy}} \quad (14a)$$

$$V_{alloy}^{FGM}(x) = 1 - V_{ceramic}^{FGM}(x). \quad (14b)$$

The Poisson's ratio [6] and coefficient of thermal expansion for the FGM may be obtained as

$$\nu(x) = \frac{\nu_{alloy} V_{alloy}^{FGM}(x) E_{ceramic} + \nu_{ceramic} V_{ceramic}^{FGM}(x) E_{alloy}}{V_{alloy}^{FGM}(x) E_{ceramic} + V_{ceramic}^{FGM}(x) E_{alloy}} \quad (15)$$

$$\gamma(x) = \gamma_{alloy} V_{alloy}^{FGM}(x) + \gamma_{ceramic} V_{ceramic}^{FGM}(x) \quad (16)$$

The fracture toughness of the FGM can be expressed as a function of the volume fraction of the ceramic [17]

$$K_{IC}(x) = \frac{K_{IC}^{alloy} + K_{IC}^{ceramic}}{2} + \frac{K_{IC}^{alloy} - K_{IC}^{ceramic}}{2} \times \left(\sqrt{1 - V_{ceramic}^{FGM}(x)} - \sqrt{V_{ceramic}^{FGM}(x)} \right) \quad (17)$$

Paris law parameters are assumed to have exponential variation as given below

$$C(x) = C_{alloy} e^{\vartheta x}, \text{ where, } \vartheta = \frac{1}{L} \ln \left(\frac{C_{ceramic}}{C_{alloy}} \right) \quad (18a)$$

$$m(x) = m_{alloy} e^{\varsigma x}, \text{ where, } \varsigma = \frac{1}{L} \ln \left(\frac{m_{ceramic}}{m_{alloy}} \right) \quad (18b)$$

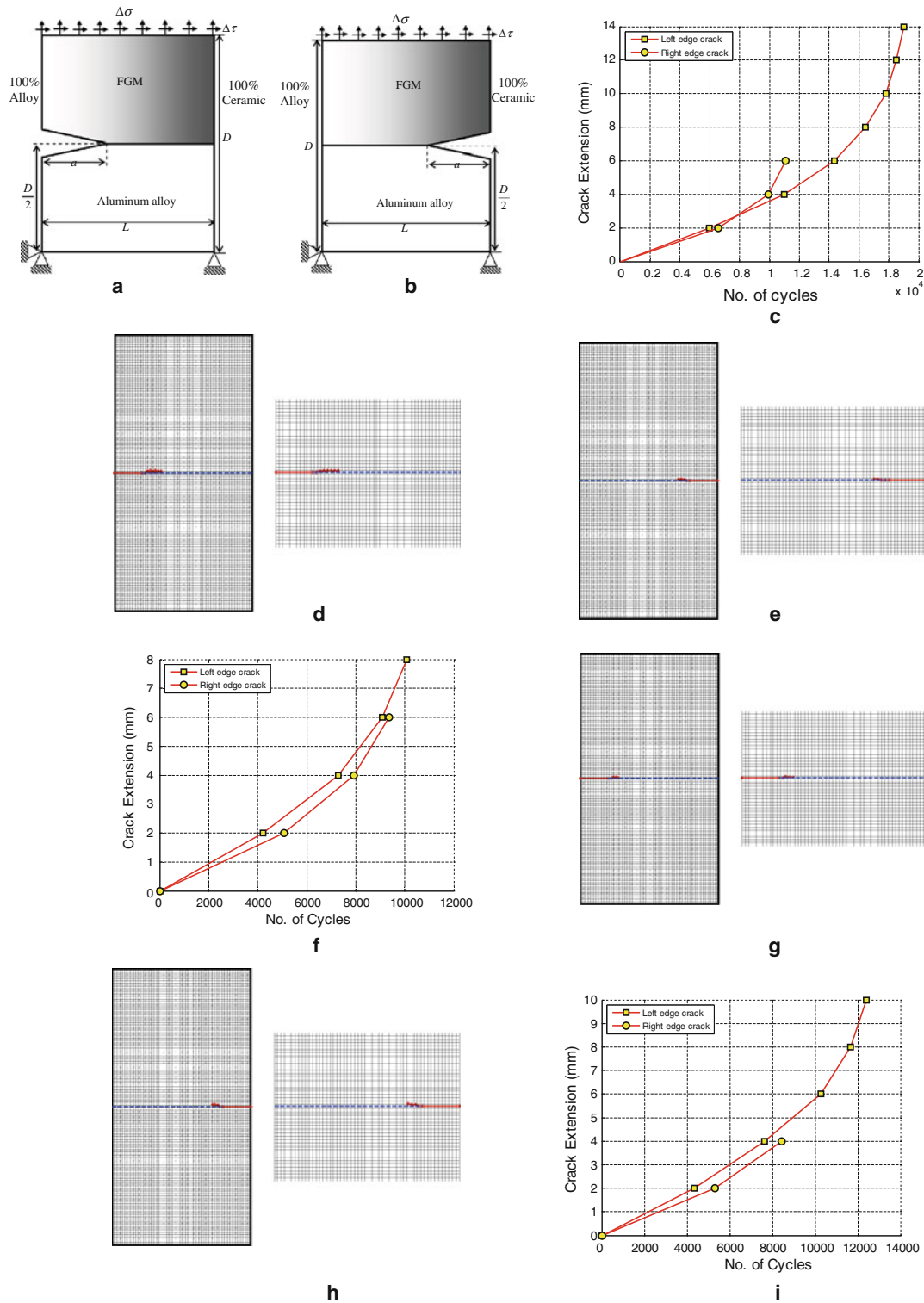


Fig. 1 **a** Left edge crack under mixed mode loading. **b** Right edge crack under mixed mode loading. **c** Edge crack extension with number of cycles under pure mode-I loading. **d** Crack path for left edge crack under pure mode-I loading. **e** Crack path for right edge crack under pure mode-I loading. **f** Edge crack extension with number of cycles under mixed-mode loading (shear load towards right). **g** Crack path for left edge crack under mixed mode loading (shear load towards right).

h Crack path for right edge crack under mixed-mode loading (shear load towards right). **i** Edge crack extension with number of cycles under mixed mode loading (shear load towards left). **j** Crack path for left edge crack under mixed mode loading (shear load towards left). **k** Crack path for right edge crack under mixed loading (shear load towards left). **l** SIFs variation under pure mode-I loading for $E_2/E_1 = 2, 10$ and 100

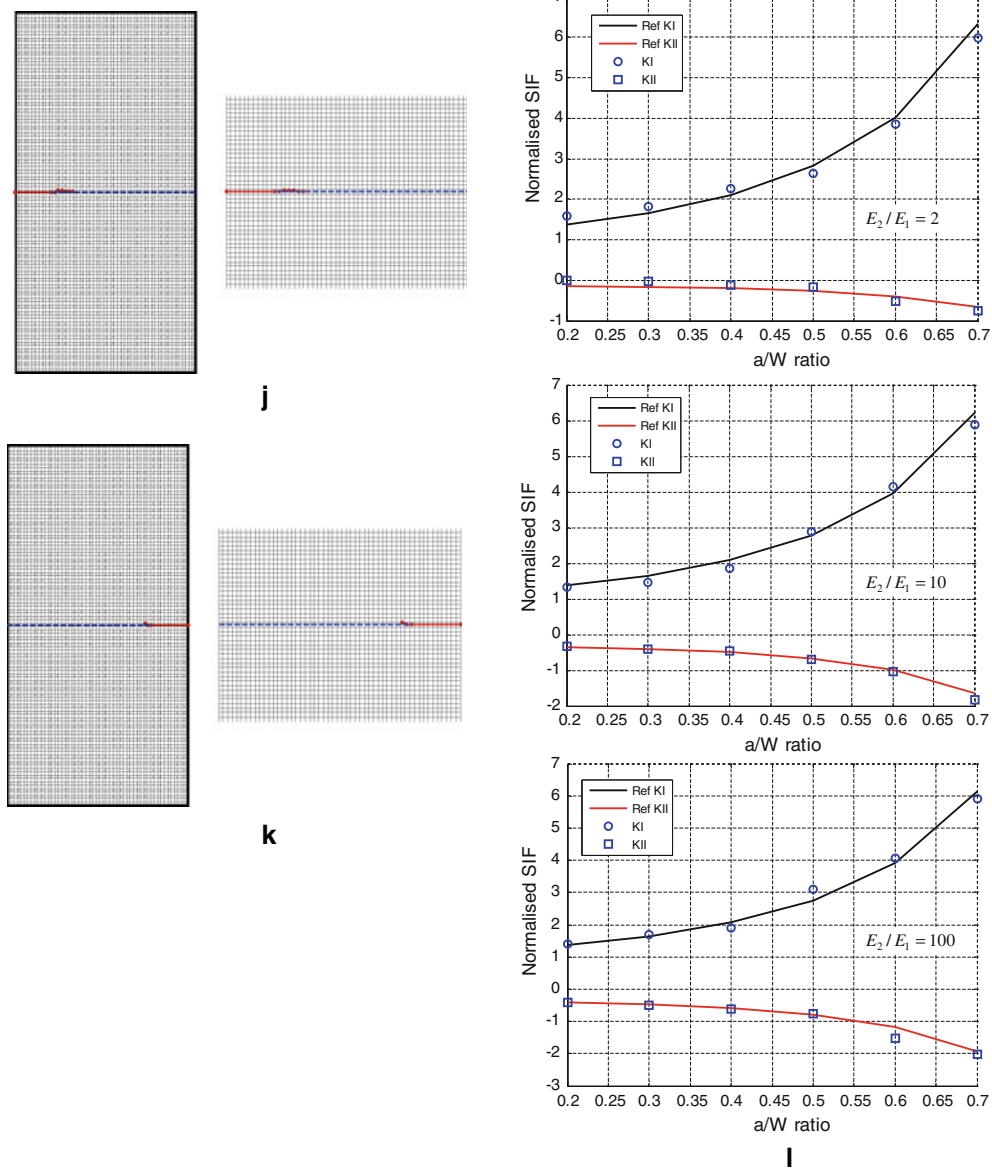


Fig. 1 continued

Table 1 Material properties of aluminum alloy and alumina [3, 20]

Material properties ^{a,b,c,d}	Aluminum alloy	Alumina
Elastic modulus E (GPa)	70	300
Poisson's ratio, ν	0.33	0.21
Coefficient of thermal expansion γ ($^{\circ}\text{C}$)	25×10^{-6}	8.2×10^{-6}
Fracture toughness K_{IC} ($\text{MPa}\sqrt{\text{m}}$)	29	3.5
Paris law parameter C in $\text{m}/\text{cycle}(\text{MPa}\sqrt{\text{m}})^{-m}$	10^{-12}	2.8×10^{-10}
Paris law parameter, m (x)	3	10

^a <http://www.efunda.com/materials/alloys/aluminum/properties.cfm>. Accessed on 27/08/2011 @ 7.06 PM.

^b <http://asm.matweb.com/search/SpecificMaterial.asp?bassnum=MA6061t6>. Accessed on 04/09/2011 @ 7.00 PM.

^c <http://accuratus.com/alumox.html>. Accessed on 27/08/2011 @ 7.08 PM.

^d http://www.coorstek.com/resources/8510-1042_Ceramic_Material_Properties.pdf. Accessed on 27/08/2011 @ 7.15 PM.

6 Problem description, results and discussions

A bi-layered plate is composed of FGM in the upper portion and aluminum alloy in the lower portion. The FGM layer consists of aluminum alloy on the left side and ceramic (alumina) on the right side. Two interface crack problems are considered i.e., an edge crack and an embedded central crack. Nine noded quadrilateral elements are used for the purpose of analysis with a regular mesh size of 107 nodes in x -direction and 215 nodes in y -direction. A plane strain condition is assumed in all the simulations. The bi-layered plate is subjected to mode-I, mixed-mode and thermal loads. In case of mode-I mechanical load, the applied fatigue load is equal to $\Delta\sigma = 70$ MPa whereas for mixed mode loading, an additional fatigue shear load of $\Delta\tau = 10$ MPa is applied at the top edge of the plate. In case of thermal loading, a temperature difference of $\Delta T = 23.86$ °C is applied to generate an equivalent mechanical load. The dimension of the domain $L = 100$ mm and $D = 200$ mm with an initial crack length of $a = 20$ mm is chosen for the simulation.

6.1 Interfacial edge crack in a finite bi-layered plate

Figure 1a, b show an interfacial edge crack in a bi-layered material on the left and the right edges respectively along with the boundary conditions. A cyclic mode-I load ($\Delta\tau = 0$) is applied at the top edge of the plates as shown in Fig. 1a, b. The plots of the number of cycles with the crack extension are presented in Fig. 1c. In this case, it is observed that the number of cycles to failure is found to be 18,742 and 10,855 for the left and right edge cracks respectively. The crack paths for this case are presented in Fig. 1d, e. From the plots of the crack paths, it is found that the crack penetrates into the upper FGM layer, and further propagates into FGM parallel to the interface for both the left and the right edge cracks.

Similarly, now the plates of bi-layered materials are subjected to mixed-mode loading as shown in Fig. 1a, b. The plots of the number of cycles with the crack extension are shown in Fig. 1f. From the results presented in Fig. 1f, it is observed that the fatigue failure life for the left and right edge crack problems is found to be 9,852 and 8,799 cycles respectively. The crack paths for the left and the right edge cracks are shown in Fig. 1g, h respectively. It is noticed that the crack propagates in the FGM for both left and right edge cracks. But the deviation in crack paths is found more as compared to mode-I loading.

Next, the bi-layered plates, shown in Fig. 1a, b, are further subjected to the mixed-mode load but the shear load ($\Delta\tau$) direction is reversed now i.e., it is acting towards left. For this type of loading, the fatigue failure cycles with crack extension are presented in Fig. 1i for the left and right edge cracks. These simulations show that the failure cycles are found to be 12,054 and 7,254 for the left and right edge

cracks respectively. The crack paths for the left and right edge cracks are presented in Fig. 1j, k respectively. From these crack paths, it is found that both cracks enter into the FGM, and keep propagating into FGM only. Similar to the previous mixed-mode load, the deviation in crack path is found more as compared to mode-I load.

To validate the results obtained by XFEM, an edge crack is taken at the interface of bi-layered plate (both layers composed of two homogeneous materials) as shown in Fig. 1a. The bi-layered plate is subjected to mode-I load of $\sigma = 100$ MPa with $\tau = 0$. The value of E_1 is taken as 70 MPa while the values of ν_1 and ν_2 are kept equal to 0.3. A plane stress condition is assumed for these simulations. Although, these results are obtained using a structured mesh but these results remain nearly the same for unstructured mesh also. The normalized values of SIF are obtained for different values of a/W ratio, and are plotted in Fig. 11 for $E_2/E_1 = 2, 10$ and 100. The results obtained by XFEM are compared with those available in literature [10]. These results show that the values of normalized SIF are found quite close to the reference values. From the results presented in these figures, it is also observed that with the increase in crack length, K_I increases while K_{II} decreases.

Now consider an edge crack lying on the left and the right edges of the plate is subjected to thermal load as shown in Fig. 2a, b. The numbers of fatigue cycles against crack extension are presented in Fig. 2c. These simulations show that the fatigue cycles for the left and right edge cracks are found to be 18,975 and 12,727 respectively. The crack paths for the left and the right edge cracks are shown in Fig. 2d, e respectively. From the crack paths, it is noticed that the crack propagates into FGM along a straight path parallel to the bi-layered interface. The deviation in crack path is found even less as compared to mode-I load.

The above simulations illustrate that the life of the interfacial edge crack plate is found maximum for thermal load whereas the life of the bi-layered plate is found minimum for mixed mode mechanical load. In addition to this, the crack propagates into FGM parallel to the bi-layered interface under cyclic thermal and mode-I mechanical load. In case of mixed mode loading, the crack penetrates into the FGM to a greater extent. This is quite obvious as the FGM is weak in fracture as compared to the aluminium alloy. Aluminium alloy possesses high uniform fracture toughness as compared to FGM. Also, the life of the FGM depends on the direction of the shear load in case of mixed-mode loading.

6.2 Interfacial central crack in a finite bi-layered plate

Consider a central crack in a finite bi-layered material plate as depicted in Fig. 3a. The upper layer consists of an FGM and the lower one is made of aluminum alloy. A mode-I cyclic load is applied at the top edge of the plate. The computed

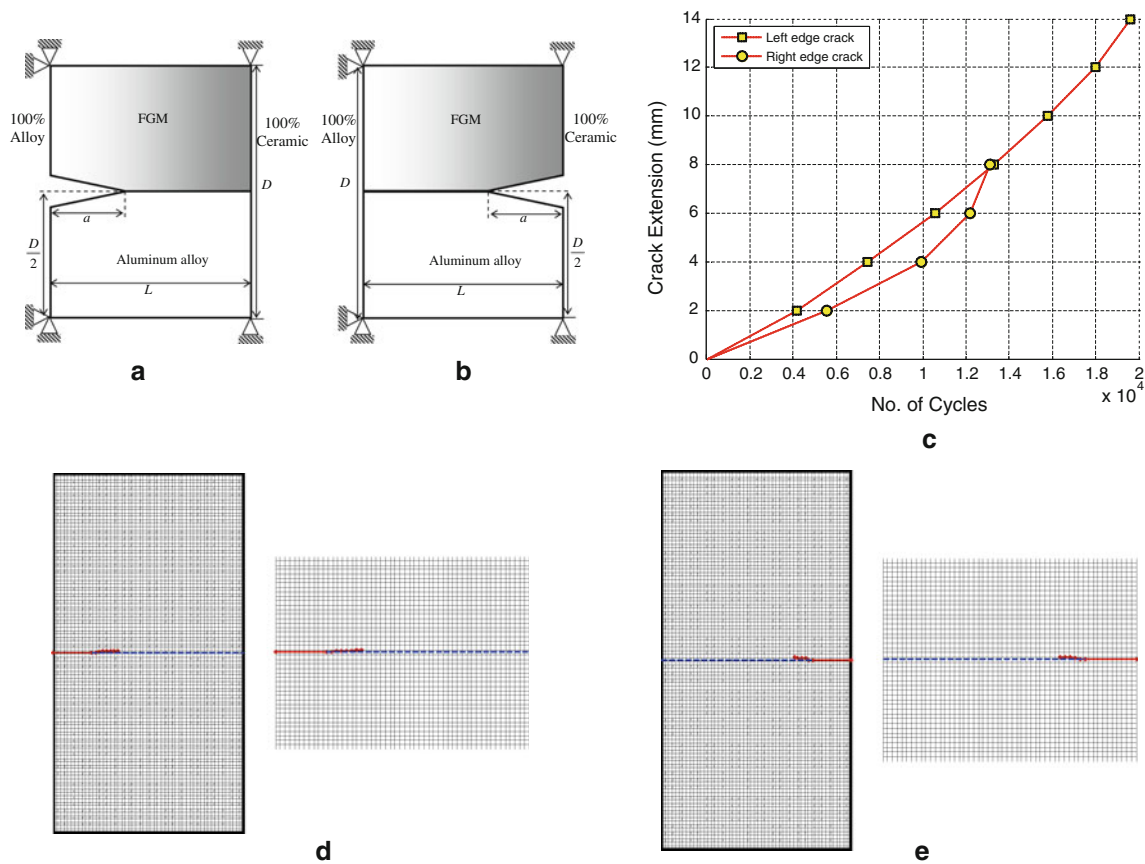


Fig. 2 **a** Left edge crack under thermal loading. **b** Right edge crack under thermal loading. **c** Edge crack extension with number of cycles under thermal loading. **d** Crack path for the left edge crack under thermal loading. **e** Crack path for right edge crack under thermal loading

results of the number of failure cycles with crack extension are presented in Fig. 3b. In this case, it is observed that the number of cycles to failure is found to be 23,115. Figure 3c shows the crack path under mode-I load. From the crack path, it is found that both crack tips propagate into FGM, and follow a straight path with minor deviation.

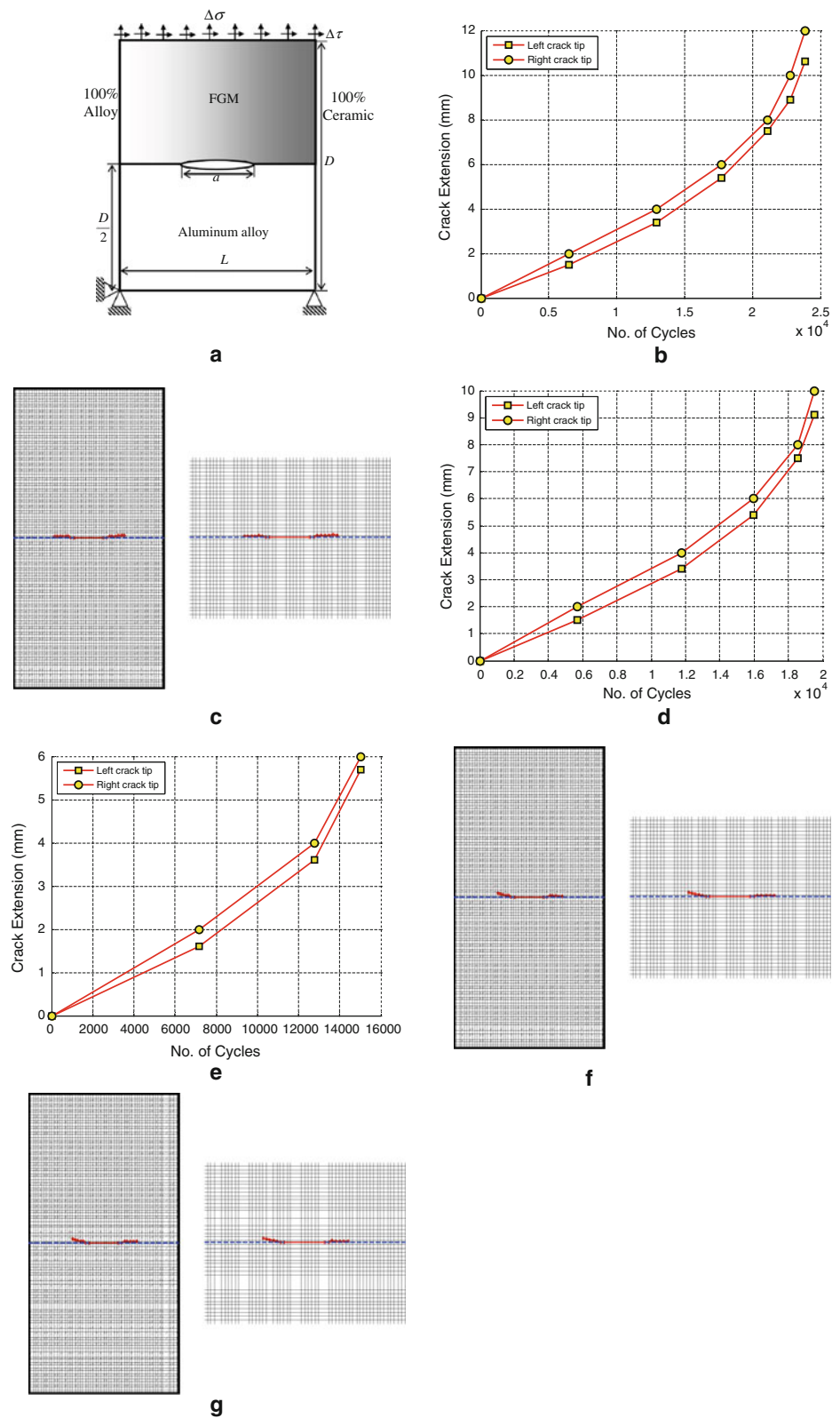
Next, a cyclic mixed-mode load is applied at the top edge of the plate as shown in Fig. 3a. In case when the shear load is acting towards the right, the fatigue cycles with crack extension are plotted in Fig. 3 whereas when the direction of shear load is reversed (acting towards left), the fatigue cycles with crack extension are shown in Fig. 3e. From these plots, the cycles to failure are found to be 18,992 and 13,052 cycles for the cases when the shear load is acting towards right and left respectively. The crack tip paths are shown in Fig. 3f for the case when shear load is acting towards right whereas the crack tip paths are shown in Fig. 3g for the case when shear load is acting towards left. From the plots of the crack tip paths, it is found that the both crack tips enter into upper FGM layer and keep on propagating into the FGM layer only. Moreover, it is observed that the

crack deviates to a significant extent under mixed mode loading.

Similarly, the plate with central crack is analysed under the cyclic thermal load as shown in Fig. 4a. In this case, the fatigue cycles with crack extension are presented in Fig. 4b. This figure shows that the fatigue failure life of the plate is found to be 30,172. The crack tip paths for this case are shown in Fig. 4c. From the crack tip paths, it is found that the central crack propagates into FGM, and follows nearly a straight path parallel to the interface. The deviation in crack tip path for this case is found even small as compared to equivalent mode-I load.

From the central interfacial crack simulations, the fatigue life of plate is found minimum under mixed-mode loading, moderate under mode-I loading, and maximum under thermal loading. Moreover, the crack propagates in FGM parallel to the interface under mode-I mechanical and thermal loads but it penetrates into FGM to greater extent under mixed-mode loading. Moreover, the life of the bi-layered plate also depends on the direction of the shear load under mixed-mode loading.

Fig. 3 **a** Central crack under mixed mode loading. **b** Central crack extension with number of cycles under pure mode-I loading. **c** Crack path for central crack under pure mode-I loading. **d** Crack extension with number of cycles when the shear load is acting towards right. **e** Crack extension with number of cycles when the shear load is acting towards left. **f** Central crack path when the shear load is acting towards right. **g** Central crack path when the shear load is acting towards left



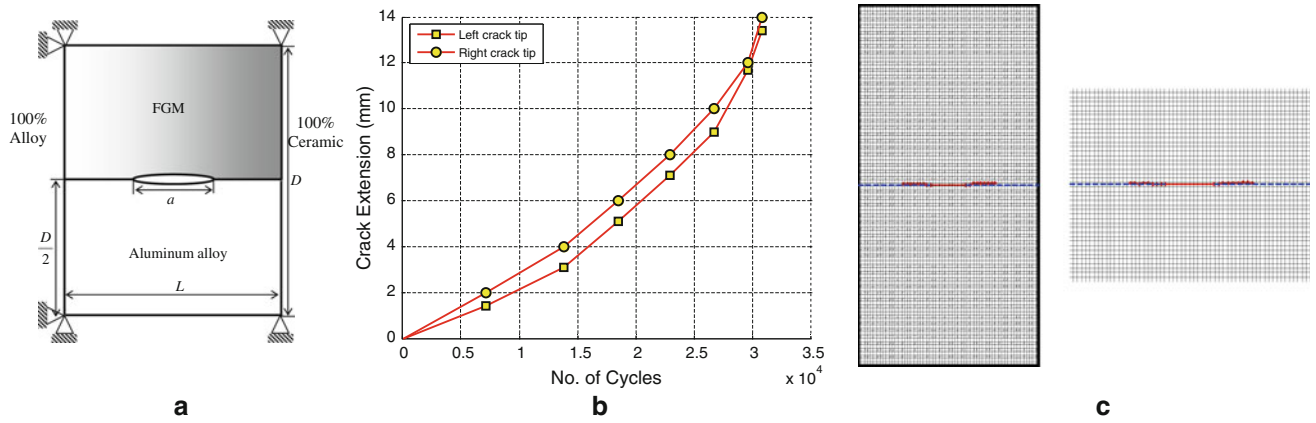


Fig. 4 a Central crack under thermal loading. b Central crack extension with number of cycles under thermal loading. c Crack path for central crack under thermal loading

7 Conclusions

An XFEM approach is developed to simulate the interfacial cracks in bi-layered materials under thermo-mechanical loads. The bi-layered plate either having an edge or a central crack at the interface is taken for the simulation. The upper part of the plate is made of FGM whereas the lower part is composed of a homogeneous material i.e., aluminum alloy. The fatigue life of the bi-layered interfacial crack is obtained for different load cases. The domain based interaction integral approach is extended to accurately evaluate the SIFs. On the basis of these simulations, it is observed that the fatigue crack propagates into the FGM for all load cases under consideration. The fatigue life of the interfacial central crack plate is found more as compared to the interfacial edge crack plate. Also, the fatigue life of the plate under mixed-mode fatigue load is found less as compared to mode-I fatigue load. It is also noticed that the fatigue life in case of equivalent thermal load is found more as compared to mode-I mechanical load. This work can be further extended to evaluate the fatigue life of the bi-layered crack plate in the presence of multiple discontinuities.

Appendix A: XFEM formulation

Governing equations

A planar domain (Ω) bounded by contour Γ divided into three parts i.e., Γ_u , Γ_t and Γ_c with internal flaws is shown in Fig. 5. The displacement boundary conditions are imposed on Γ_u , while tractions are applied on Γ_t and traction free condition are imposed on crack surfaces Γ_c . The equilibrium and boundary conditions for this problem may be described as

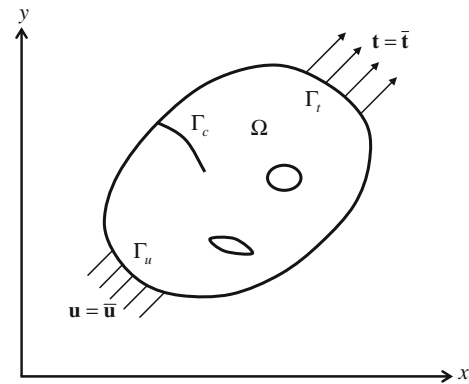


Fig. 5 Domain with discontinuities

$$\nabla \cdot \sigma + \mathbf{b} = \mathbf{0} \text{ in } \Omega \tag{19a}$$

$$\sigma \cdot \hat{\mathbf{n}} = \bar{\mathbf{t}} \text{ on } \Gamma_t \tag{19b}$$

$$\sigma \cdot \hat{\mathbf{n}} = \mathbf{0} \text{ on } \Gamma_c \tag{19c}$$

$$\mathbf{u} = \hat{\mathbf{u}} \text{ on } \Gamma_u \tag{19d}$$

where σ is the Cauchy stress tensor, \mathbf{u} is the displacement field vector, \mathbf{b} is the body force vector per unit volume, $\bar{\mathbf{t}}$ is the external traction vector and $\hat{\mathbf{n}}$ is the unit outward normal vector. For small displacements, strain-displacement relation can be described as

$$\boldsymbol{\varepsilon} = \boldsymbol{\varepsilon}(\mathbf{u}) = \nabla_s \mathbf{u} \tag{20}$$

where ∇_s is the symmetric part of the gradient operator.

The constitutive relations for the linear elastic FGM under consideration is given by Hook’s law

$$\sigma(\mathbf{u}) = D(\mathbf{x}) : \boldsymbol{\varepsilon}(u) \tag{21a}$$

where \mathbf{x} is the vector of x and y -coordinates, $D(\mathbf{x})$ is the constitutive matrix, which can be written for plane strain condition as

$$D(\mathbf{x}) = \frac{E(\mathbf{x})}{\{1 - 2\nu(\mathbf{x})\} \{1 + \nu(\mathbf{x})\}} \times \begin{bmatrix} 1 - \nu(\mathbf{x}) & \nu(\mathbf{x}) & 0 \\ \nu(\mathbf{x}) & 1 - \nu(\mathbf{x}) & 0 \\ 0 & 0 & \frac{1-2\nu(\mathbf{x})}{2} \end{bmatrix} \quad (21b)$$

Variational formulation

Let the space for admissible displacement fields λ be defined by Moes et al. [11]

$$\lambda = (\mathbf{v} \in \delta | \mathbf{v} = \bar{\mathbf{u}} \text{ on } \Gamma_u) \text{ and } \mathbf{v} \text{ discontinuous on } \Gamma_c \quad (22a)$$

where the space δ is related to the regularity of the solution. In the same way, the test function space λ_0 may be defined as

$$\lambda_0 = (\mathbf{v} \in \delta | \mathbf{v} = 0 \text{ on } \Gamma_u) \text{ and } \mathbf{v} \text{ discontinuous on } \Gamma_c \quad (22b)$$

A weak form of the equilibrium equation can be written as

$$\int_{\Omega} \boldsymbol{\sigma}(\mathbf{u}) : \boldsymbol{\varepsilon}(\mathbf{v}) d\Omega = \int_{\Omega} \mathbf{b} \cdot \mathbf{v} d\Omega + \int_{\Gamma_t} \bar{\mathbf{t}} \cdot \mathbf{v} d\Gamma \quad (23)$$

Substituting the constitutive relation $\boldsymbol{\sigma}(\mathbf{u}) = D(\mathbf{x}) : \boldsymbol{\varepsilon}(\mathbf{u})$ in the above equation, we obtain

$$\int_{\Omega} \boldsymbol{\varepsilon}(\mathbf{u}) : D(\mathbf{x}) : \boldsymbol{\varepsilon}(\mathbf{v}) d\Omega = \int_{\Omega} \mathbf{b} \cdot \mathbf{v} d\Omega + \int_{\Gamma_t} \bar{\mathbf{t}} \cdot \mathbf{v} d\Gamma \quad (24)$$

The linear form, \widehat{T} and the bilinear form, \widehat{S} of the above equation are obtained as

$$\widehat{T}(\mathbf{v}) = \int_{\Gamma} \mathbf{b} \cdot \mathbf{v} d\Omega + \int_{\Gamma_t} \bar{\mathbf{t}} \cdot \mathbf{v} d\Omega \quad (25)$$

$$\widehat{S}(\mathbf{u}, \mathbf{v}) = \int_{\Omega} \boldsymbol{\varepsilon}(\mathbf{u}) : D(\mathbf{x}) : \boldsymbol{\varepsilon}(\mathbf{v}) d\Omega \quad (26)$$

The quadratic energy functional can be written as

$$\Pi(\mathbf{u}) = \frac{1}{2} \widehat{S}(\mathbf{u}, \mathbf{u}) - \widehat{T}(\mathbf{u}) \quad (27)$$

On substitution of the relevant quantities, the expression for the same is obtained as

$$\Pi(\mathbf{u}) = \frac{1}{2} \int_{\Omega} \boldsymbol{\varepsilon}(\mathbf{u}) : D(\mathbf{x}) : \boldsymbol{\varepsilon}(\mathbf{u}) d\Omega - \int_{\Gamma} \mathbf{b} \cdot \mathbf{u} d\lambda - \int_{\Gamma_t} \bar{\mathbf{t}} \cdot \mathbf{u} d\lambda \quad (28)$$

By substituting the trial and test functions and taking variation of the above equation, the following set of discrete equations is obtained using the arbitrariness of nodal variations

$$[\mathbf{K}] \{\mathbf{d}\} = \{\mathbf{f}\} \quad (29)$$

where \mathbf{d} is the vector of nodal unknowns, \mathbf{K} and \mathbf{f} are the global stiffness matrix and the external force vector respectively. The stiffness matrix and force vector are computed on element level, and are assembled into their global counterparts through usual finite element assembly procedure.

Displacement approximation

For modeling cracks in XFEM [4, 11], the approximation function takes the following form

$$\mathbf{u}^h(\mathbf{x}) = \sum_{i=1}^n N_i(\mathbf{x}) \left[\bar{\mathbf{u}}_i + \underbrace{H(\mathbf{x}) \mathbf{a}_i}_{i \in n_r} + \underbrace{\sum_{j=1}^4 \beta_j(\mathbf{x}) \mathbf{b}_i^j}_{i \in n_A} \right] \quad (30a)$$

where i is the set of all nodes in the domain, $N_i(\mathbf{x})$ is the element shape function associated with node i satisfying the partition of unity criterion, $\bar{\mathbf{u}}_i$ is the nodal displacement vector associated with the continuous part of the finite element solution, \mathbf{a}_i denotes the additional unknown degrees of freedom associated with the discontinuous Heaviside function $H(\mathbf{x})$, and is defined for those elements, which are completely cut by the crack to account for the jump in the displacement field, \mathbf{b}_i^j is the additional degrees of freedom associated with those elements, which are partially cut by the crack, and accounts for stress singularity at the crack tip, n is the set of all nodes in the mesh, n_r is the set of nodes belonging to those elements which are completely cut by the crack, and n_A is the set of nodes belonging to those elements which are partially cut by the crack. In Eq. (30a), the first term represents the standard finite element approximation, the second term represents the enrichment for those elements which are completely cut by the crack, and the third term represents the enrichment for those elements which contain the crack tip. For any node n_r , Heaviside jump function, $H(\mathbf{x})$ takes a constant value, and is equal to +1 on one side and -1 on other side of the crack. Also, the standard displacements do not correspond to the displacements computed by XFEM. Thus, a shifted enrichment is used. If \mathbf{x}_i is the node of interest then Eq. (30a) can be written as

$$\mathbf{u}^h(\mathbf{x}) = \sum_{i=1}^n N_i(\mathbf{x}) \left[\bar{\mathbf{u}}_i + \underbrace{[\mathbf{H}(\mathbf{x}) - H(\mathbf{x}_i)]\mathbf{a}_i}_{i \in n_r} + \underbrace{\sum_{j=1}^4 [\beta_j(\mathbf{x}) - \beta_j(\mathbf{x}_i)]\mathbf{b}_i^j}_{i \in n_A} \right] \tag{30b}$$

In Eq. (30b), the difference between the values of the Heaviside function at the evaluation (Gauss) point and nodal point is taken to maintain the partition of unity. The tip enrichment is performed for those elements which contain the crack tip, and is achieved by adding additional function derived from the theory of linear elastic fracture mechanics available in the literature [2].

For isotropic and bi-layered FGM, the crack tip enrichment functions are same as that of the homogenous materials [14], and are obtained from the displacement solution of a linear elastic crack in the infinite plate [2].

$$\beta_j(\mathbf{x}) = \left[\sqrt{r} \sin \frac{\theta}{2}, \sqrt{r} \cos \frac{\theta}{2}, \sqrt{r} \cos \frac{\theta}{2} \sin \theta, \sqrt{r} \sin \frac{\theta}{2} \sin \theta \right] \tag{30c}$$

XFEM formulation for cracks in FGM

Using the approximation function defined in Eq. (30b) for a crack, the elemental matrices, \mathbf{K}^e and \mathbf{f}^e are obtained as

$$\mathbf{f}^e = \left\{ \mathbf{f}_i^u \quad \mathbf{f}_i^a \quad \mathbf{f}_i^{b1} \quad \mathbf{f}_i^{b2} \quad \mathbf{f}_i^{b3} \quad \mathbf{f}_i^{b4} \right\}^T \text{ and} \tag{31a}$$

$$\mathbf{K}_{ij}^e = \begin{bmatrix} K_{ij}^{uu} & K_{ij}^{ua} & K_{ij}^{ub} \\ K_{ij}^{au} & K_{ij}^{aa} & K_{ij}^{ab} \\ K_{ij}^{bu} & K_{ij}^{ba} & K_{ij}^{bb} \end{bmatrix} \tag{31a}$$

The sub-matrices and vectors that appear in the foregoing equations are given by

$$\mathbf{K}_{ij}^{rs} = \int_{\Omega^e} (\mathbf{B}_i^r)^T \mathbf{D} \mathbf{B}_j^s d\Omega \quad \text{where, } r, s = u, a, b \tag{31b}$$

$$\mathbf{f}_i^u = \int_{\Omega^e} N_i \mathbf{b} d\Omega + \int_{\Gamma_t} N_i \bar{\mathbf{t}} d\Gamma \tag{31c}$$

$$\mathbf{f}_i^a = \int_{\Omega^e} N_i (H(\mathbf{x}) - H(\mathbf{x}_i)) \mathbf{b} d\Omega + \int_{\Gamma_t} N_i (H(\mathbf{x}) - H(\mathbf{x}_i)) \bar{\mathbf{t}} d\Gamma \tag{31d}$$

$$\mathbf{f}_i^{b\hat{\alpha}} = \int_{\Omega^e} N_i \beta_{\hat{\alpha}}((\mathbf{x}) - (\mathbf{x}_i)) \mathbf{b} d\Omega$$

$$+ \int_{\Gamma_t} N_i (\beta_{\hat{\alpha}}(\mathbf{x}) - (\mathbf{x}_i)) \bar{\mathbf{t}} d\Gamma \quad \text{where, } \hat{\alpha} = 1, 2, 3, 4 \tag{31e}$$

where N_i are finite element shape function, \mathbf{B}_i^u , \mathbf{B}_i^a , \mathbf{B}_i^b and $\mathbf{B}_i^{b\hat{\alpha}}$ are the matrices of shape function derivatives given by

$$\mathbf{B}_i^u = \begin{bmatrix} N_{i,x} & 0 \\ 0 & N_{i,y} \\ N_{i,y} & N_{i,x} \end{bmatrix} \tag{31f}$$

$$\mathbf{B}_i^a = \begin{bmatrix} (N_i(H(\mathbf{x}) - H(\mathbf{x}_i)))_{,x} & 0 \\ 0 & (N_i(H(\mathbf{x}) - H(\mathbf{x}_i)))_{,y} \\ (N_i(H(\mathbf{x}) - H(\mathbf{x}_i)))_{,y} & (N_i(H(\mathbf{x}) - H(\mathbf{x}_i)))_{,x} \end{bmatrix} \tag{31g}$$

$$\mathbf{B}_i^{b\hat{\alpha}} = \begin{bmatrix} (N_i(\beta_{\hat{\alpha}}(\mathbf{x}) - \beta_{\hat{\alpha}}(\mathbf{x}_i)))_{,x} & 0 \\ 0 & (N_i(\beta_{\hat{\alpha}}(\mathbf{x}) - \beta_{\hat{\alpha}}(\mathbf{x}_i)))_{,y} \\ (N_i(\beta_{\hat{\alpha}}(\mathbf{x}) - \beta_{\hat{\alpha}}(\mathbf{x}_i)))_{,y} & (N_i(\beta_{\hat{\alpha}}(\mathbf{x}) - \beta_{\hat{\alpha}}(\mathbf{x}_i)))_{,x} \end{bmatrix}, \tag{31h}$$

$\hat{\alpha} = 1, 2, 3, 4$

After obtaining the numerical formulations, Eq. (29) is solved to obtain the nodal displacements, and then strains and stresses are evaluated through post-processing. The difference between the solution for a homogenous material and FGM lies in the fact that the material properties are a function of the space variable. After obtaining the values of stress and strain components, the values of stress intensity factor are evaluated using domain based interaction integral approach.

Appendix B: Computation of stress intensity factors for FGMS

For an elastic body subjected to thermo-mechanical load (Fig. 6), a quantity J' (equivalent to J -integral) is given by

$$J' = \oint_{\Gamma_o} \left(\tilde{W} \delta_{1j} - \sigma_{ij} \frac{\partial u_i}{\partial x_1} \right) n_j d\Gamma \tag{32}$$

where $\mathbf{x} = [x_1 \quad x_2]^T \equiv [x \quad y]^T$, \tilde{W} is the strain energy density function and n_j is the j th component of the outward unit vector normal to an arbitrary closed contour Γ_o enclosing the area A_o . The J' in Eq. (32) can be converted into domain form using divergence theorem,

$$J' = \int_{A_o} \left(\frac{\partial \tilde{W}}{\partial x_1} - \frac{\partial \sigma_{ij}}{\partial x_j} \frac{\partial u_i}{\partial x_1} - \sigma_{ij} \frac{\partial^2 u_i}{\partial x_1 \partial x_j} \right) dA \tag{33}$$

In Eq. (33), $\frac{\partial \sigma_{ij}}{\partial x_j} \frac{\partial u_i}{\partial x_1} = 0$ from equilibrium equations. For a linear elastic material subjected to thermo-mechanical load, \tilde{W} can be written as

$$\tilde{W} = \frac{1}{2} \sigma_{ij} \varepsilon_{ij}^m = \frac{1}{2} C_{ijkl} \varepsilon_{kl}^m \varepsilon_{ij}^m \tag{34a}$$

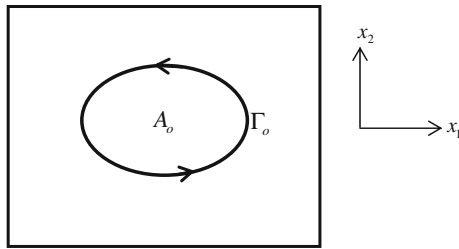


Fig. 6 Path Γ_o surrounding an enclosed area A_o

where, $\varepsilon_{ij}^m = \varepsilon_{ij} - \gamma \Delta T \delta_{ij}$ (34b)

γ is the coefficient of thermal expansion and ΔT is the temperature difference. Now from Eq. (34a), we get

$$\frac{\partial \tilde{W}}{\partial x_1} = \frac{1}{2} \frac{\partial C_{ijkl}}{\partial x_1} \varepsilon_{kl}^m \varepsilon_{ij}^m + \sigma_{ij} \frac{\partial \varepsilon_{ij}^m}{\partial x_1}$$
 (34c)

From Eq. (34b), we get $\frac{\partial \varepsilon_{ij}^m}{\partial x_1} = \frac{\partial \varepsilon_{ij}}{\partial x_1} - \frac{\partial \gamma}{\partial x_1} \Delta T \delta_{ij} - \gamma \frac{\partial \Delta T}{\partial x_1} \delta_{ij}$
 Now, Eq. (34c) becomes

$$\begin{aligned} \frac{\partial \tilde{W}}{\partial x_1} &= \frac{1}{2} \frac{\partial C_{ijkl}}{\partial x_1} \varepsilon_{kl}^m \varepsilon_{ij}^m + \sigma_{ij} \frac{\partial \varepsilon_{ij}}{\partial x_1} \\ &\quad - \sigma_{ij} \left(\gamma \frac{\partial \Delta T}{\partial x_1} + \frac{\partial \gamma}{\partial x_1} \Delta T \right) \delta_{ij} \end{aligned}$$
 (34d)

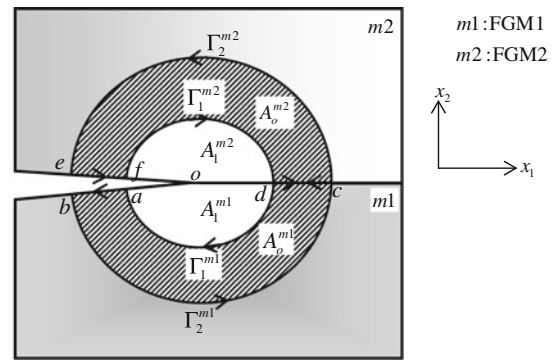
Substituting $\frac{\partial \tilde{W}}{\partial x_1}$ from Eq. (34d) into Eq. (33), we arrive at,

$$J' = \int_{A_o} \left(\frac{1}{2} \frac{\partial C_{ijkl}}{\partial x_1} \varepsilon_{ij}^m \varepsilon_{kl}^m - \sigma_{kk} \frac{\partial(\gamma \Delta T)}{\partial x_1} \right) dA$$
 (34e)

Hence,

$$\begin{aligned} J' &= \oint_{\Gamma_o} \left(\tilde{W} \delta_{1j} - \sigma_{ij} \frac{\partial u_i}{\partial x_1} \right) n_j d\Gamma \\ &= \int_{A_o} \left(\frac{1}{2} \frac{\partial C_{ijkl}}{\partial x_1} \varepsilon_{ij}^m \varepsilon_{kl}^m - \sigma_{kk} \frac{\partial(\gamma \Delta T)}{\partial x_1} \right) dA \end{aligned}$$
 (35)

Now consider bi-material cracked body consisting of two functionally graded materials as shown in Fig. 7. The crack is lying at the interface of two materials along x -axis. For an enclosed area A_o^{m1} surrounded by a closed path ($a \rightarrow b \rightarrow \Gamma_2^{m1} \rightarrow c \rightarrow d \rightarrow \Gamma_1^{m1}$) as shown in Fig. 7, Eq. (35) can be rewritten as



A_1 = area enclosed by $o \rightarrow f \rightarrow \Gamma_1^{m2} \rightarrow d \rightarrow \Gamma_1^{m1} \rightarrow a \rightarrow o = A_1^{m2} + A_1^{m1}$
 A_2 = area enclosed by $o \rightarrow a \rightarrow b \rightarrow \Gamma_2^{m1} \rightarrow c \rightarrow \Gamma_2^{m2} \rightarrow e \rightarrow f \rightarrow o = A_2^{m1} + A_2^{m2}$

Fig. 7 Path independent closed contour around the crack tip

$$\begin{aligned} J'_1 &= \int_{ab} \left(\tilde{W} \delta_{1j} - \sigma_{ij} \frac{\partial u_i}{\partial x_1} \right) n_j d\Gamma \\ &\quad + \int_{\Gamma_2^{m1}} \left(\tilde{W} \delta_{1j} - \sigma_{ij} \frac{\partial u_i}{\partial x_1} \right) n_j d\Gamma \\ &\quad + \int_{cd} \left(\tilde{W} \delta_{1j} - \sigma_{ij} \frac{\partial u_i}{\partial x_1} \right) n_j d\Gamma \\ &\quad + \int_{\Gamma_1^{m1}} \left(\tilde{W} \delta_{1j} - \sigma_{ij} \frac{\partial u_i}{\partial x_1} \right) n_j d\Gamma \\ &= \int_{A_o^{m1}} \left(\frac{1}{2} \frac{\partial C_{ijkl}}{\partial x_1} \varepsilon_{ij}^m \varepsilon_{kl}^m - \sigma_{kk} \frac{\partial(\gamma \Delta T)}{\partial x_1} \right) dA \end{aligned}$$
 (36)

Similarly, for an enclosed area A_o^{m2} as shown in Fig. 7 surrounded by a closed path2 ($d \rightarrow c \rightarrow \Gamma_2^{m2} \rightarrow e \rightarrow f \rightarrow \Gamma_1^{m2}$), Eq. (36) can be written as

$$\begin{aligned} J'_2 &= \int_{dc} \left(\tilde{W} \delta_{1j} - \sigma_{ij} \frac{\partial u_i}{\partial x_1} \right) n_j d\Gamma \\ &\quad + \int_{\Gamma_2^{m2}} \left(\tilde{W} \delta_{1j} - \sigma_{ij} \frac{\partial u_i}{\partial x_1} \right) n_j d\Gamma \\ &\quad + \int_{ef} \left(\tilde{W} \delta_{1j} - \sigma_{ij} \frac{\partial u_i}{\partial x_1} \right) n_j d\Gamma \\ &\quad + \int_{\Gamma_1^{m2}} \left(\tilde{W} \delta_{1j} - \sigma_{ij} \frac{\partial u_i}{\partial x_1} \right) n_j d\Gamma \\ &= \int_{A_o^{m2}} \left(\frac{1}{2} \frac{\partial C_{ijkl}}{\partial x_1} \varepsilon_{ij}^m \varepsilon_{kl}^m - \sigma_{kk} \frac{\partial(\gamma \Delta T)}{\partial x_1} \right) dA \end{aligned}$$
 (37)

Let $\widehat{F} = \left(\widetilde{W}\delta_{1j} - \sigma_{ij} \frac{\partial u_i}{\partial x_1} \right)$ and $\widehat{G} = \left(\frac{1}{2} \frac{\partial C_{ijkl}}{\partial x_1} \varepsilon_{ij}^m \varepsilon_{kl}^m - \sigma_{kk} \frac{\partial(\gamma \Delta T)}{\partial x_1} \right)$. Now combining Eqs. (36) and (37), we get

$$\begin{aligned}
 J' &= \int_{ab} \widehat{F} n_j d\Gamma + \int_{\Gamma_2^{m1}} \widehat{F} n_j d\Gamma + \int_{cd} \widehat{F} n_j d\Gamma \\
 &+ \int_{\Gamma_1^{m1}} \widehat{F} n_j d\Gamma + \int_{dc} \widehat{F} n_j d\Gamma \\
 &+ \int_{\Gamma_2^{m2}} \widehat{F} n_j d\Gamma + \int_{ef} \widehat{F} n_j d\Gamma \\
 &+ \int_{\Gamma_1^{m2}} \widehat{F} n_j d\Gamma = \int_{A_o^{m1}} \widehat{G} dA + \int_{A_o^{m2}} \widehat{G} dA \quad (38)
 \end{aligned}$$

where $J' = J'_1 + J'_2$. If $\Gamma_1 = \Gamma_1^{m1} + \Gamma_1^{m2}$, $\Gamma_2 = \Gamma_2^{m1} + \Gamma_2^{m2}$, $A_1 = A_1^{m1} + A_1^{m2}$, $A_2 = A_2^{m1} + A_2^{m2}$, $A_o^{m1} = A_2^{m1} - A_1^{m1}$, $A_o^{m2} = A_2^{m2} - A_1^{m2}$, $A_o = A_2 - A_1 = A_o^{m1} + A_o^{m2}$, then Eq. (38) reduces to

$$\begin{aligned}
 J' &= \int_{ab} \widehat{F} n_j d\Gamma + \int_{\Gamma_2} \widehat{F} n_j d\Gamma + \int_{cd} \widehat{F} n_j d\Gamma + \int_{\Gamma_1} \widehat{F} n_j d\Gamma \\
 &+ \int_{dc} \widehat{F} n_j d\Gamma + \int_{ef} \widehat{F} n_j d\Gamma = \int_{A_o} \widehat{G} dA \quad (39)
 \end{aligned}$$

In Eq. (39), $\int_{ab} \widehat{F} n_j d\Gamma = 0$ and $\int_{ef} \widehat{F} n_j d\Gamma = 0$ as $\sigma_{ij} n_j = 0$, and $\widetilde{W}\delta_{1j} n_j d\Gamma = \widetilde{W} dx_2 = 0$.

Moreover, $\int_{cd} \widehat{F} n_j d\Gamma + \int_{dc} \widehat{F} n_j d\Gamma = 0$ as $\widetilde{W}\delta_{1j} n_j d\Gamma = 0$ and $\sigma_{ij} n_j \frac{\partial u_i}{\partial x_1}$ is continuous across the perfect interface between two functionally graded materials. Finally Eq. (39) reduces to

$$\begin{aligned}
 J' &= \int_{\Gamma_2} \left(\widetilde{W}\delta_{1j} - \sigma_{ij} \frac{\partial u_i}{\partial x_1} \right) n_j d\Gamma \\
 &+ \int_{\Gamma_1} \left(\widetilde{W}\delta_{1j} - \sigma_{ij} \frac{\partial u_i}{\partial x_1} \right) n_j d\Gamma \\
 &= \int_{A_o} \left(\frac{1}{2} \frac{\partial C_{ijkl}}{\partial x_1} \varepsilon_{ij}^m \varepsilon_{kl}^m - \sigma_{kk} \frac{\partial(\gamma \Delta T)}{\partial x_1} \right) dA \quad (40)
 \end{aligned}$$

Since, $A_o = A_2 - A_1$ and changing the direction of arrow on Γ_1 , above equation reduces to

$$\begin{aligned}
 &\int_{\Gamma_2} \left(\widetilde{W}\delta_{1j} - \sigma_{ij} \frac{\partial u_i}{\partial x_1} \right) n_j d\Gamma \\
 &- \int_{\Gamma_1} \left(\widetilde{W}\delta_{1j} - \sigma_{ij} \frac{\partial u_i}{\partial x_1} \right) n_j d\Gamma \\
 &+ \int_{A_2 - A_1} \left(\sigma_{kk} \frac{\partial(\gamma \Delta T)}{\partial x_1} - \frac{1}{2} \frac{\partial C_{ijkl}}{\partial x_1} \varepsilon_{ij}^m \varepsilon_{kl}^m \right) dA = 0 \quad (41)
 \end{aligned}$$

Equation (41) can be further simplified as

$$\begin{aligned}
 &\int_{\Gamma_2} \left(\widetilde{W}\delta_{1j} - \sigma_{ij} \frac{\partial u_i}{\partial x_1} \right) n_j d\Gamma \\
 &+ \int_{A_2} \left(\sigma_{kk} \frac{\partial(\gamma \Delta T)}{\partial x_1} - \frac{1}{2} \frac{\partial C_{ijkl}}{\partial x_1} \varepsilon_{ij}^m \varepsilon_{kl}^m \right) dA \\
 &= \int_{\Gamma_1} \left(\widetilde{W}\delta_{1j} - \sigma_{ij} \frac{\partial u_i}{\partial x_1} \right) n_j d\Gamma \\
 &+ \int_{A_1} \left(\sigma_{kk} \frac{\partial(\gamma \Delta T)}{\partial x_1} - \frac{1}{2} \frac{\partial C_{ijkl}}{\partial x_1} \varepsilon_{ij}^m \varepsilon_{kl}^m \right) dA \quad (42)
 \end{aligned}$$

Hence, for a bi-layered material of two FGMs having a crack and an interface both along x_1 -direction, the integral $J = \int_{\Gamma} \left(\widetilde{W}\delta_{1j} - \sigma_{ij} \frac{\partial u_i}{\partial x_1} \right) n_j d\Gamma - \int_A \left(\frac{1}{2} \frac{\partial C_{ijkl}}{\partial x_1} \varepsilon_{ij}^m \varepsilon_{kl}^m - \sigma_{kk} \frac{\partial(\gamma \Delta T)}{\partial x_1} \right) dA$ is path independent, where Γ is a path starting from the lower crack face and terminating on the upper crack face and A is the enclosed area within Γ .

Further, let q be a weight function such that its value is *one* at the inner path Γ_1 , zero at the outer path Γ_2 , and arbitrary elsewhere. Now J can be written as

$$\begin{aligned}
 J &= \int_{\Gamma_1} \widehat{F} n_j d\Gamma - \int_{A_1} \widehat{G} dA \\
 &= - \int_{\Gamma_2} \widehat{F} n_j q d\Gamma - \int_{ef} \widehat{F} n_j q d\Gamma + \int_{\Gamma_1} \widehat{F} n_j q d\Gamma \\
 &- \int_{ab} \widehat{F} n_j q d\Gamma - \int_{A_1} \widehat{G} dA \quad (43)
 \end{aligned}$$

where first integral is zero because $q = 0$ on Γ_2 , and second and fourth integrals are also zero because the integrands are zero on the crack faces. Eq. (43) can be written as

$$J = - \oint_{A_1} \widehat{F} q n_j d\Gamma - \int_{A_1} \widehat{G} dA \quad (44)$$

where first term in Eq. (44) represents a closed contour enclosing the area A_o , and A_1 represents the enclosed area inside the contour Γ_1 . In order to enhance the usefulness of J , the form of contour integral is converted to equivalent domain form as

$$J = - \int_{A_o} \frac{\partial}{\partial x_j} \{ \widehat{F} q \} dA - \int_{A_1} \widehat{G} dA \tag{45a}$$

where A_o is an enclosed area inside the closed contour in Eq. (45a). Let the weight function q takes a value one at the crack tip and zero at the contour Γ_2 . If inner contour Γ_1 shrink to the crack tip then $A_1 = 0$, $A_o = A_2$, and Eq. (45a) may be simplified to

$$J = - \int_{A_o} \frac{\partial}{\partial x_j} \{ \widehat{F} q \} dA \tag{45b}$$

After substituting the value of \widehat{F} , Eq. (45b) can be written as

$$J = \int_{A_o} \frac{\partial}{\partial x_j} \left\{ \left(\sigma_{ij} \frac{\partial u_i}{\partial x_1} - \widetilde{W} \delta_{1j} \right) q \right\} dA \tag{46}$$

For calculating the interaction integral for an elastic body, we consider two equilibrium states of the cracked body. State 1 is the actual state with given boundary conditions while state 2 is an auxiliary state. Superscript a represents the parameters for auxiliary state.

Actual state (State 1):	σ_{ij}	ε_{ij}	u_i	ΔT	\widetilde{J}
Auxiliary state (State 2):	σ_{ij}^a	ε_{ij}^a	u_i^a	0	J^a

Defining thermal J - integral for both states

$$\widetilde{J} = \int_{A_o} \frac{\partial}{\partial x_j} \left\{ \left(\sigma_{ij} \frac{\partial u_i}{\partial x_1} - \frac{1}{2} \sigma_{ik} \varepsilon_{ik}^m \delta_{1j} \right) q \right\} dA \tag{47a}$$

$$J^a = \int_{A_o} \frac{\partial}{\partial x_j} \left\{ \left(\sigma_{ij}^a \frac{\partial u_i^a}{\partial x_1} - \frac{1}{2} \sigma_{ik}^a \varepsilon_{ik}^a \delta_{1j} \right) q \right\} dA \tag{47b}$$

The J -integral for the two superimposed state will be given as

$$J_T = \int_{A_o} \frac{\partial}{\partial x_j} \left\{ \left((\sigma_{ij} + \sigma_{ij}^a) \left(\frac{\partial u_i}{\partial x_1} + \frac{\partial u_i^a}{\partial x_1} \right) - \frac{1}{2} (\sigma_{ik} + \sigma_{ik}^a) (\varepsilon_{ik}^m + \varepsilon_{ik}^a) \delta_{1j} \right) q \right\} dA \tag{47c}$$

$$J_T = \widetilde{J} + J^a + M_{12} \tag{48}$$

where

$$M_{12} = \int_{A_o} \frac{\partial}{\partial x_j} \left\{ \left(\sigma_{ij} \frac{\partial u_i^a}{\partial x_1} + \sigma_{ij}^a \frac{\partial u_i}{\partial x_1} - \frac{1}{2} (\sigma_{ik} \varepsilon_{ik}^a + \sigma_{ik}^a \varepsilon_{ik}^m) \delta_{1j} \right) q \right\} dA \tag{49}$$

where the auxiliary field for the FGM may be taken from Yu et al. [24,25] as

$$\sigma_{ij}^a = C_{ijkl}^{tip} \frac{1}{2} \left(\frac{\partial u_k^a}{\partial x_l} + \frac{\partial u_l^a}{\partial x_k} \right), \varepsilon_{ij}^a = S_{ijkl}(\mathbf{x}) \sigma_{kl}^a \text{ and } \varepsilon_{ij}^a \neq \frac{1}{2} \left(\frac{\partial u_i^a}{\partial x_j} + \frac{\partial u_j^a}{\partial x_i} \right) \tag{50}$$

Using the following $\sigma_{ik} \varepsilon_{ik}^a = \sigma_{ik} S_{ikpq}(\mathbf{x}) \sigma_{pq}^a = \varepsilon_{pq}^m \sigma_{pq}^a = \sigma_{ik}^a \varepsilon_{ik}^m$, Eq. (49) can be written as

$$M_{12} = \int_{A_o} \frac{\partial}{\partial x_j} \left\{ \left(\sigma_{ij} \frac{\partial u_i^a}{\partial x_1} + \sigma_{ij}^a \frac{\partial u_i}{\partial x_1} - \sigma_{ik}^a \varepsilon_{ik}^m \delta_{1j} \right) q \right\} dA \tag{51}$$

Equation (51) can be modified as

$$M_{12} = \int_{A_o} \left(\sigma_{ij} \frac{\partial u_i^a}{\partial x_1} + \sigma_{ij}^a \frac{\partial u_i}{\partial x_1} - \sigma_{ik}^a \varepsilon_{ik}^m \delta_{1j} \right) \frac{\partial q}{\partial x_j} dA + \int_{A_o} \frac{\partial}{\partial x_j} \left(\sigma_{ij} \frac{\partial u_i^a}{\partial x_1} + \sigma_{ij}^a \frac{\partial u_i}{\partial x_1} - \sigma_{ik}^a \varepsilon_{ik}^m \delta_{1j} \right) q dA \tag{52}$$

Equation (52) can be written as

$$M_{12} = \int_{A_o} \left(\sigma_{ij} \frac{\partial u_i^a}{\partial x_1} + \sigma_{ij}^a \frac{\partial u_i}{\partial x_1} - \sigma_{ik}^a \varepsilon_{ik}^m \delta_{1j} \right) \frac{\partial q}{\partial x_j} dA + \int_{A_o} \left(\frac{\partial \sigma_{ij}}{\partial x_j} \frac{\partial u_i^a}{\partial x_1} + \sigma_{ij} \frac{\partial^2 u_i^a}{\partial x_j \partial x_1} + \frac{\partial \sigma_{ij}^a}{\partial x_j} \frac{\partial u_i}{\partial x_1} + \sigma_{ij}^a \frac{\partial^2 u_i}{\partial x_j \partial x_1} - \frac{\partial \sigma_{ik}^a}{\partial x_1} \varepsilon_{ik}^m - \sigma_{ik}^a \frac{\partial \varepsilon_{ik}^m}{\partial x_1} \right) q dA \tag{53}$$

Using equilibrium equation, $\frac{\partial \sigma_{ij}}{\partial x_j} \frac{\partial u_i^a}{\partial x_1} = 0$, and $\frac{\partial \sigma_{ij}^a}{\partial x_j} \frac{\partial u_i}{\partial x_1} = 0$. Due to symmetry of the stress tensor, $\sigma_{ij} \frac{\partial^2 u_i^a}{\partial x_j \partial x_1} = \sigma_{ij} \frac{1}{2} \frac{\partial}{\partial x_1} \left(\frac{\partial u_i^a}{\partial x_j} + \frac{\partial u_j^a}{\partial x_i} \right)$ and $\sigma_{ij}^a \frac{\partial^2 u_i}{\partial x_j \partial x_1} = \sigma_{ij}^a \frac{\partial \varepsilon_{ij}}{\partial x_1}$. Finally Eq. (52) is simplified as

$$M_{12} = \int_{A_o} \left(\sigma_{ij} \frac{\partial u_i^a}{\partial x_1} + \sigma_{ij}^a \frac{\partial u_i}{\partial x_1} - \sigma_{ik}^a \varepsilon_{ik}^m \delta_{1j} \right) \frac{\partial q}{\partial x_j} dA + \int_{A_o} \left(\sigma_{ij} \frac{1}{2} \frac{\partial}{\partial x_1} \left(\frac{\partial u_i^a}{\partial x_j} + \frac{\partial u_j^a}{\partial x_i} \right) + \sigma_{ij}^a \frac{\partial}{\partial x_1} \left(\varepsilon_{ij} - \varepsilon_{ij}^m \right) - \frac{\partial \sigma_{ik}^a}{\partial x_1} \varepsilon_{ik}^m \right) q dA \tag{54}$$

Using Eq. (50), Eq. (54) can be further simplified as

$$\begin{aligned}
 M_{12} = & \int_{A_o} \left(\sigma_{ij} \frac{\partial u_i^a}{\partial x_1} + \sigma_{ij}^a \frac{\partial u_i}{\partial x_1} - \sigma_{ik}^a \varepsilon_{ik}^m \delta_{1j} \right) \frac{\partial q}{\partial x_j} dA \\
 & + \int_{A_o} \left(\sigma_{ij} \left(S_{ijkl}^{tip} - S_{ijkl}(\mathbf{x}) \right) \frac{\partial \sigma_{kl}^a}{\partial x_1} \right. \\
 & \left. + \sigma_{ij}^a \left(\frac{\partial \gamma}{\partial x_1} \Delta T + \gamma \frac{\partial \Delta T}{\partial x_1} \right) \delta_{ij} \right) q dA \quad (55)
 \end{aligned}$$

References

- Amit KC, Kim JH (2008) Interaction integrals for thermal fracture of functionally graded materials. *Eng Frac Mech* 75:2542–2565
- Anderson TL (1995) *Fracture mechanics: fundamentals and applications*. CRC Press, Florida. ISBN 0-8493-4260-0
- Arola D, Huang MP, Sultan MB (1999) The failure of amalgam dental restorations due to cyclic fatigue crack growth. *J Mater Sci Mater Med* 10:319–327
- Belytschko T, Black T (1999) Elastic crack growth in finite elements with minimal remeshing. *Int J Numer Methods Eng* 45:601–620
- Guo L, Guo F, Yu H, Zhang L (2012) An interaction energy integral method for nonhomogeneous materials with interfaces under thermal loading. *Int J Solids Struct* 49:355–365
- Hsieh CL, Tuang WH (2005) Poisson's ratio of two phase composites. *Mat Sci Eng A* 396:202–205
- Kim JH, Paulino GH (2005) Consistent formulations of the interaction integral method for fracture of functionally graded materials. *J Appl Mech* 72:351–364
- Liu XY, Xiao QZ, Karihaloo BL (2004) XFEM for direct evaluation of mixed mode SIFs in homogeneous and bi-materials. *Int J Numer Methods Eng* 59:1103–1118
- Menshykov OV, Menshykova MV, Guz IA (2012) 3-D elastodynamic contact problem for an interface crack under harmonic loading. *Eng Frac Mech* 80:52–59
- Miyakazi N, Ikeda T, Soda T, Munakata T (1993) Stress intensity factor analysis of interface crack using boundary element method—application of contour-integral method. *Eng Frac Mech* 45:599–610
- Moes N, Dolbow J, Belytschko T (1999) A finite element method for crack growth without remeshing. *Int J Numer Methods Eng* 46:131–150
- Nagai M, Ikeda T, Miyazaki N (2007) Stress intensity factor analysis of a three-dimensional interface crack between dissimilar anisotropic materials. *Eng Frac Mech* 74:2481–2497
- Pant M, Singh IV, Mishra BK (2011) Evaluation of mixed mode stress intensity factors for interface cracks using EFGM. *Appl Math Model* 35:3443–3459
- Pathak H, Singh A, Singh IV (2012) Numerical simulation of bi-material interfacial cracks using EFGM and XFEM. *Int J Mech Mater Design* 8:9–36
- Qin TY, Zhu BJ, Noda NA (2008) Mixed-mode stress intensity factors of a three-dimensional crack in a bonded biomaterial. *Eng Comput* 25:251–267
- Rao BN, Rahman S (2003) Meshfree analysis of cracks in isotropic functionally graded materials. *Eng Frac Mech* 70:1–27
- Raveendran KV, Verma AP, Rao CVSK (1991) Effective fracture toughness of composites. *Int J Frac* 47:R63–R65
- Rethore J, Gravouil A, Combescure A (2005a) An energy-conserving scheme for dynamic crack growth using the extended finite element method. *Int J Numer Methods Eng* 63:631–659
- Rethore J, Gravouil A, Combescure A (2005b) A combined space-time extended finite element method. *Int J Numer Methods Eng* 64:260–284
- Roylance D (2001) *Fatigue*. Department of Materials Science and Engineering, Massachusetts Institute of Technology, Cambridge
- Sukumar N, Prevost J (2003) Modeling quasi-static crack growth with the extended finite element method part I: computer implementation. *Int J Solids Struct* 40:7513–7537
- Sukumar N, Huang ZY, Prevost J, Suo Z (2004) Partition of unity enrichment for bi-material interface cracks. *Int J Numer Methods Eng* 59:1075–1102
- Walters MC, Paulino GH (2006) Computation of mixed-mode stress intensity factors for cracks in three-dimensional functionally graded solids. *J Eng Mech* 132:1–15
- Yu H, Wu L, Guo L, He Q, Du S (2010a) Interaction integral method for the interfacial fracture problems of two non-homogeneous materials. *Mech Mat* 42:435–450
- Yu H, Wu L, Guo L, Wu H, Du S (2010b) An interaction integral method for 3D curved cracks in nonhomogeneous materials with complex interfaces. *Int J Solids Struct* 47:2178–2189
- Zhu B, Shi Y, Qin T, Sukop M, Yu S, Li Y (2009) Mixed-mode stress intensity factors of 3D interface crack in fully coupled electro-magneto-thermoelastic multiphase composites. *Int J Solids Struct* 46:2669–2679